Synthesis of Dispersible Ferromagnetic Graphene Nanoribbon Stacks with Enhanced Electrical Percolation Properties in a Magnetic Field

Bostjan Genorio,[†,⊥,∥] Zhiwei Peng,[†] Wei Lu,[†] B. Katherine Price Hoelscher,[¶] Barbara Novosel,[⊥,∥] and James M. Tour[†,‡,§,*]

[†]Department of Chemistry, [‡]Department of Mechanical Engineering and Materials Science, and [§]Richard E. Smalley Institute for Nanoscale Science and Technology, Rice University, 6100 Main Street, Houston, Texas 77005, United States, [⊥]Centre of Excellence for Low-Carbon Technologies, Hajdrihova 19, 1000 Ljubljana, Slovenia, [∥]Faculty of Chemistry and Chemical Technology, University of Ljubljana, Aškerčeva cesta 5, 1000 Ljubljana, Slovenia, and [¶]M-I SWACO, 5950 North Course Drive, Houston, Texas 77072, United States

ABSTRACT Iron-intercalated and tetradecyl-edge-functionalized graphene nanoribbon stacks (Fe@TD-GNRs) can be made from commercially available carbon nanotubes by a facile synthesis. The physical properties of the Fe@TD-GNRs were analyzed by transmission electron microscopy, thermogravimetric analysis, X-ray photoelectron spectroscopy, evolved gas analysis, Raman spectroscopy, and scanning electron microscopy. By the intercalation of iron, the alignment of the Fe@TD-GNRs in a magnetic field was enabled. The aligned structures enhanced electrical percolation at given concentrations in previously nonconductive solvents.

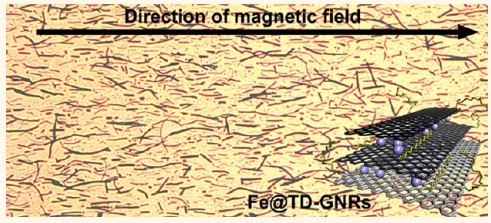

KEYWORDS: graphene nanoribbons · electrical percolation · intercalated graphene · ferromagnetic

Graphene-based nanomaterials have attracted wide attention due to their promise for use in industrial applications. This is spawned from the extraordinary electrical, mechanical, and thermal properties of graphene materials.[1] Focusing mainly on the electrical properties, graphene nanoribbons (GNRs) can be seen as future candidates for applications in energy-related devices,[2] catalysis, transparent touch screens,[3] carbon fiber spinning and coating,[4] polymer composites, and various oilfield drilling, completion, and logging fluids.[5] The electronic-related advantages that GNRs have over other carbon allotropes are their potential for anisotropic alignment, while maintaining surface areas that exceed that of carbon nanotubes (CNTs). When considering GNRs as electronic conductors in various applications, the potential for alignment is of great importance since bulk conductivity can be achieved at lower concentrations. Depending on the length-to-width ratio and their edge states, GNRs can behave as semiconductors[6] or electrical conductors.[7] GNRs have been synthesized by the longitudinal unzipping of multiwalled carbon nanotubes (MWCNTs) using oxidative conditions followed by chemical reduction.[8] Such oxidation/reduction procedures leave irreversible defects on the GNR basal planes and consequently lower their electrical conductivity. This problem can be mitigated by the splitting of MWCNTs with vapor phase intercalation of potassium followed by alcohol quenching, which yields more highly conductive GNRs.[7] To date, the unzipping of MWCNTs is considered to be the method of choice for a bulk preparation of GNRs, and the process has been used by many.[9−12] Other methods of GNR synthesis have been reported, including formation of GNRs within single-walled carbon nanotubes (SWCNTs).[13]

If GNRs are to be used in bulk quantities with high enough conductivity for the requisite applications, then facile processability is required. The edge-selective functionalization of GNRs produces such a material, as previously shown by the one-pot splitting of MWCNTs followed by *in situ* functionalization,

* Address correspondence to tour@rice.edu.

Received for review September 28, 2012 and accepted October 31, 2012.

Published online October 31, 2012
10.1021/nn304509c

a "wet" chemistry approach.[14] Although single ribbons are conductive materials, the bulk conductivity might differ considerably as a percolation network must be formed. It is known that electrical percolation is concentration-dependent for isotropic materials such as spheres. Electrical percolation for high aspect ratio materials, such as anisotropic CNTs, is both concentration- and alignment-dependent. Carbon nanotube polymer composites are a widely studied system that exhibit electrical percolation.[15] Calculations have shown that the highest conductivity at a fixed concentration of CNTs can be achieved if they are partially aligned.[16] The question that follows is, how can one align less rigid anisotropic particles such as GNRs? While it would be convenient to exploit the intrinsic magnetism of GNRs, this property is functional only in very controlled and structurally perfect systems such as zigzag-edged GNRs. The presence of edge defects drastically destabilizes the intrinsic magnetism.[17] One possibility is to make a liquid-crystalline phase of GNRs, a procedure that is used for fiber spinning.[18] Or, as we investigate here, one might align GNRs in magnetic fields through surface deposition of magnetic nanoparticles.[19] Since GNR stacks are 2D analogues of CNTs, it is reasonable to expect a similar behavior between the two regarding electrical percolation. Further, intuitively, it is expected that the contacts between GNR stacks are better than contacts between CNTs since more $\pi-\pi$ interactions of the flat GNR surfaces are likely; however, this conjecture has not been experimentally confirmed.

We report here the synthesis and intercalation of ferromagnetic materials, such as iron, between the planes of GNR stacks. GNR stacks are by definition graphite analogues. Graphite materials are known to form graphite intercalation compounds (GICs) with various intercalants, including iron.[20,21] As a similar intercalation behavior is expected for GNRs, iron-intercalated GNR stacks should additionally exhibit an anisotropic response to an external magnetic field, yielding an aligned architecture. If the alignment is to be formed in the liquid phase, it is necessary to have highly dispersible ferromagnetic GNRs. Dispersibility can be achieved by edge functionalization[14] while not sacrificing magnetic properties and electronic conductivity. Further, bulk alignment in the liquid phase at a fixed concentration is expected to enhance the electrical percolation threshold (make the requisite concentration of GNRs lower). A material with dispersibility, conductivity, and anisotropic response to an external magnetic field can be valuable in a variety of applications where conductivity is desired while minimizing the carbon additive.

RESULTS AND DISCUSSION

Synthesis. Iron(III) chloride ($FeCl_3$) is known to intercalate between graphene layers to form graphite intercalation compounds.[20−22] It has also been shown that $FeCl_3$ can be intercalated between the layered tubular structure of MWCNTs.[23] $FeCl_3$ was intercalated into the bundles of commercially available MWCNTs (Scheme 1). For this purpose, a two-compartment glass tube was used; the MWCNTs were loaded into one compartment, and $FeCl_3$ was added to the second compartment. The tube, set on its side, was then vacuum-sealed and heated at 350 °C for 1 day. The $FeCl_3$-intercalated MWCNTs ($FeCl_3$@MWCNTs) were then subjected to hydrolysis with water vapor at 110 °C for 1 day. During hydrolysis, the $FeCl_3$ formed oxides, complexes, and hydrolytic polymers.[24] The intercalated Fe was then reduced to elemental Fe in a H_2 atmosphere at 800 °C for 1 h, yielding Fe-intercalated MWCNTs (Fe@MWCNTs). The last step of the reaction was the one-pot splitting followed by edge functionalization[14] that yielded the final product: iron-intercalated tetradecyl-edge-functionalized graphene nanoribbon stacks (Fe@TD-GNRs). This procedure is shown as route 1 in Scheme 1. An attempt to optimize the procedure for Fe@TD-GNRs is shown in route 2 of Scheme 1. In the first step, we prepared $FeCl_3$@MWCNTs as described above. $FeCl_3$@MWCNTs were then treated with electride (Na/K alloy in 1,2-dimethoxyethane (1,2-DME)) to reduce Fe^{3+} to Fe, split the MWCNTs, and activate edges of newly formed GNRs. The reaction mixture was quenched with 1-iodotetradecane to functionalize the edges of GNRs. The Na/K alloy treatment step was a one-pot reaction. However, as it will be shown later, the iron content of the product from route 2 was not high; route 3 (Scheme 1) was then devised to increase the iron content. In route 3, the MWCNTs were first split to yield GNR stacks. In the next step, the GNRs were intercalated with $FeCl_3$ using the same procedure as for intercalation of $FeCl_3$ into MWCNT bundles. The product of the second step was $FeCl_3$@GNRs. We hypothesize that $FeCl_3$ could intercalate between graphene layers more easily since the structure is more open at the edges when compared to MWCNTs. The third step of route 3 was the one-pot reduction of the $FeCl_3$ and the tetradecyl edge functionalization of the GNRs, yielding Fe@TD-GNRs. MeOH was used to quench all of the Na/K reactions after splitting and/or alkylation. The final edge alkylation is harder to envision by this third route since formation of exclusive edge deprotonation is unlikely. Therefore, much of the material is likely intercalated as we have shown previously.[14]

The final product, Fe@TD-GNRs, synthesized using route 3 was imaged by transmission electron microscopy (TEM). Dark dots represent iron nanoparticles that could be intercalated between graphene layers (Figure 1). In the images, the edges of the Fe@TD-GNRs can be clearly seen.

Thermogravimetric Analysis (TGA). To estimate the concentration of iron in the product, the Fe@TD-GNRs were analyzed by TGA in air. The concentration of iron

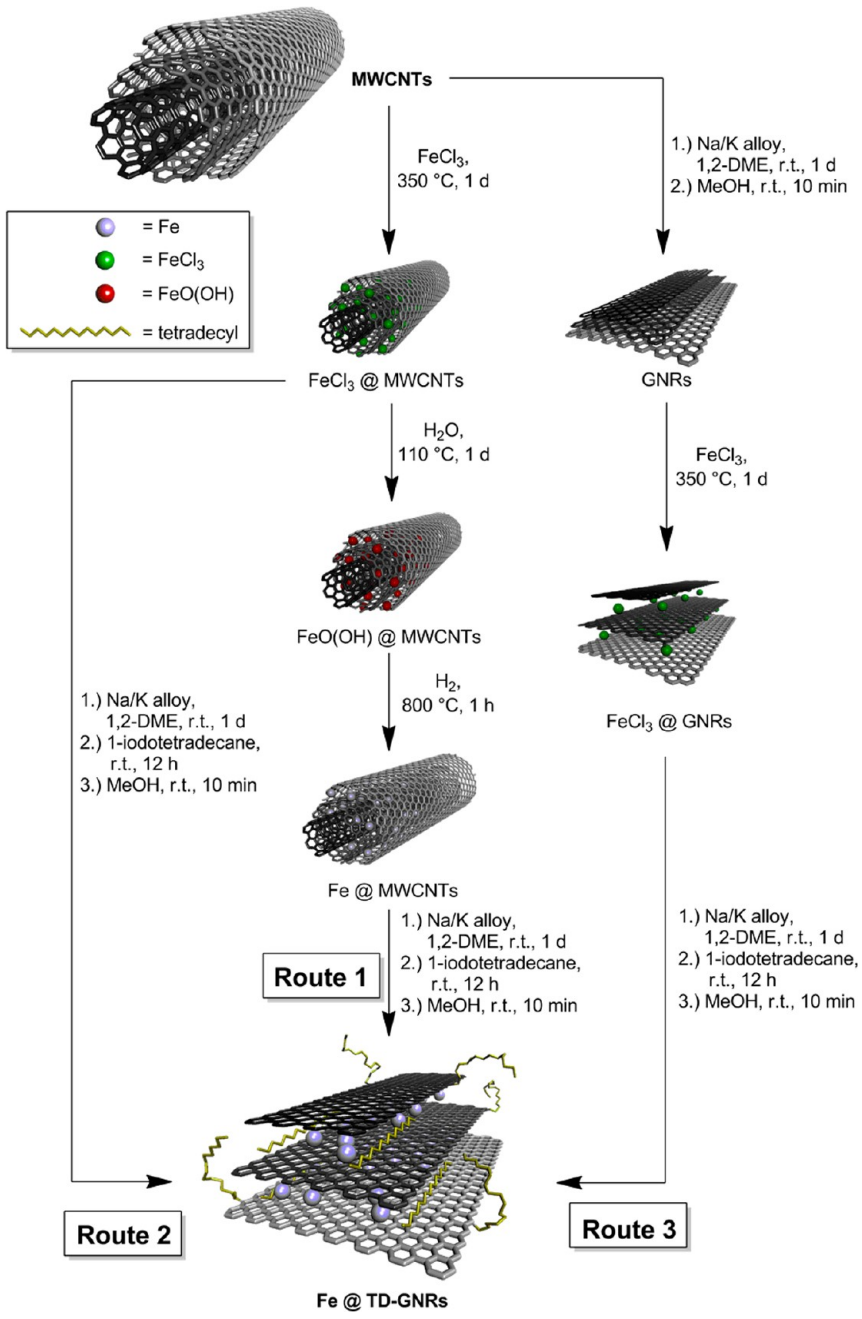

Scheme 1. Proposed reaction schemes route 1, route 2, and route 3 for the synthesis of iron-intercalated tetradecylated graphene nanoribbons (Fe@TD-GNRs) as described in the text.

was calculated from the thermolysis residue, assuming the residue was Fe_2O_3. The TGA results are summarized in Figure 2a. Mitsui-originated Fe@TD-GNRs had an iron content of 12.9 wt % (route 1), 4.2 wt % (route 2), and 29.5 wt % (route 3). The results indicate that GNRs (route 3) are more suitable precursors for the intercalation of iron, as the iron concentration was much higher than in the case of MWCNTs (route 1 and route 2). Since the MWCNTs are split to GNRs before intercalation in route 3, more sites are introduced where iron can be intercalated between graphene layers. Control TGA of pristine MWCNTs produced a minimum amount of the inorganic residue, indicating that most of the iron was intercalated and not derived from the catalyst used to make the MWCNTs.

X-ray Photoelectron Spectroscopy (XPS). XPS was also used to estimate the iron content of the Fe@TD-GNR samples. Concentrations were measured in atomic % (at %) and were between 0 at % for Fe@GNRs synthesized according to route 1 and route 2 and 1 at % for Fe@GNRs synthesized according to route 3 (Figure 2b). The concentrations by XPS were much lower than the concentrations estimated from TGA; the Fe@TD-GNRs synthesized according to route 3 again showed the

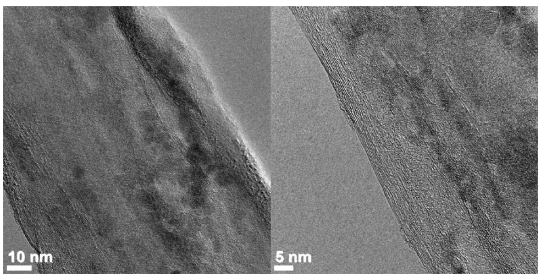

Figure 1. TEM images of Fe@TD-GNRs synthesized according to route 3.

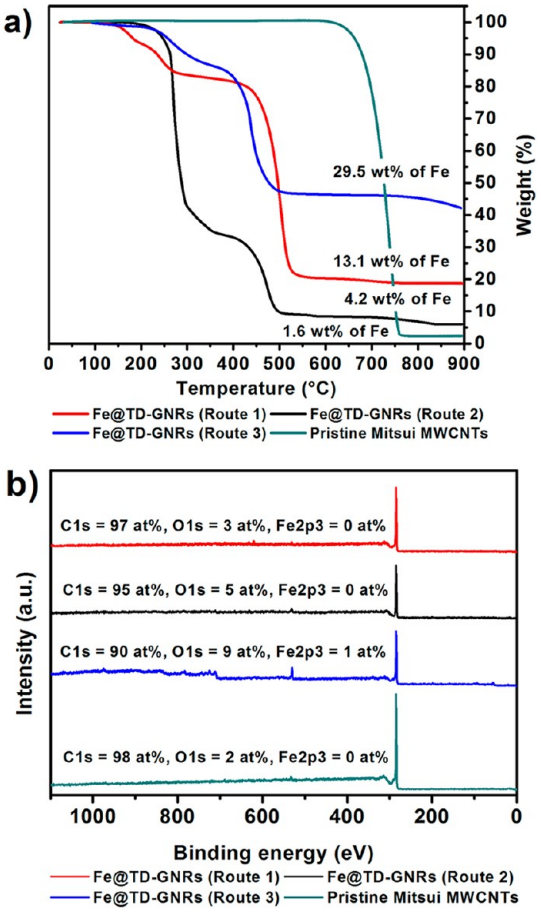

Figure 2. Estimation of the iron concentration in Fe@TD-GNRs synthesized according to routes 1−3. (a) TGA plots recorded in a dynamic air flow with a heating rate of 10 °C/min. (b) XPS spectra of the same Fe@TD-GNR samples from routes 1−3. No residual chlorine was observed using the XPS survey technique.

highest iron concentration at 1 at %. That corresponds to 4.4 wt % of iron, which is much less than 29.5 wt % estimated from TGA. This result may be an indication that iron is indeed intercalated and not adsorbed on the surface, as one might expect. XPS is a surface technique where the typical depth of analysis is 3−5 nm. We know from our previous studies[14] that GNRs synthesized using Na/K alloy are usually ~30 nm thick. Considering this fact, we conclude that the iron is primarily intercalated and not at the surface. Deconvolution of the Fe

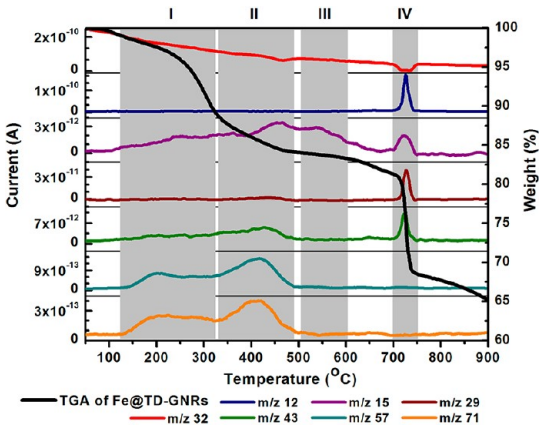

Figure 3. Evolved gas analysis for Fe@TD-GNRs synthesized according to route 3. The black curve represents the TGA profile of Fe@TD-GNRs recorded in dynamic argon flow with a heating rate of 10 °C/min. The colored curves represent fragments with *m/z* typical for alkane fragmentation, except for the red curve that represents the *m/z* that corresponds to oxygen. Gray rectangles are crudely selected regions for different thermodynamic profiles.

$2p_{3/2}$ spectral line (not shown) indicates that, in addition to the main signal at 707 eV [the signal that is characteristic of Fe(0)], signals at 710.5 and 713 eV were also present. Those signals most likely correspond to oxidized iron, Fe_2O_3 and/or Fe_3O_4.

Evolved Gas Analysis (EGA). We have previously shown that EGA is a sensitive technique that reveals the qualitative nature of the functional group: whether they are physisorbed or chemisorbed.[14] The Fe@TD-GNRs with the highest iron concentration, synthesized according to route 3, were analyzed (Figure 3). As for the previously described alkylated GNRs,[14] at least three distinct temperature ranges were determined in which the alkyl groups could be present in the off-gas from thermolysis products: region I between 125 and 330 °C, region II between 330 and 490 °C, and region III between 500 and 600 °C. In regions I and II, gases with *m/z* 15, 43, 57, and 71 were evolved, corresponding to alkyl fragments, while region III has only one distinctive evolved gas with *m/z* 15, which corresponds to methyl groups. Weight losses for these three regions are 10.3% for region I, 4.6% for region II, and 0.7% for region III. These results are similar to those from the previous study;[14] therefore, it was concluded that the process in region I is the deintercalation of alkanes or alkenes and in region II and region III constitutes the defunctionalization of tetradecyl groups. However, the EGA analysis of Fe@TD-GNRs produced a fourth region that is narrow and pronounced for fragments with *m/z* 12, 15, 29, and 43. This process is characteristic for these iron-intercalated functionalized GNRs while not present in functionalized GNRs without the iron. There are two interesting characteristics of the process in region IV: a high and narrow temperature range and sharp weight loss. This is an indication of a rapid process. An *m/z* 32, which corresponds to

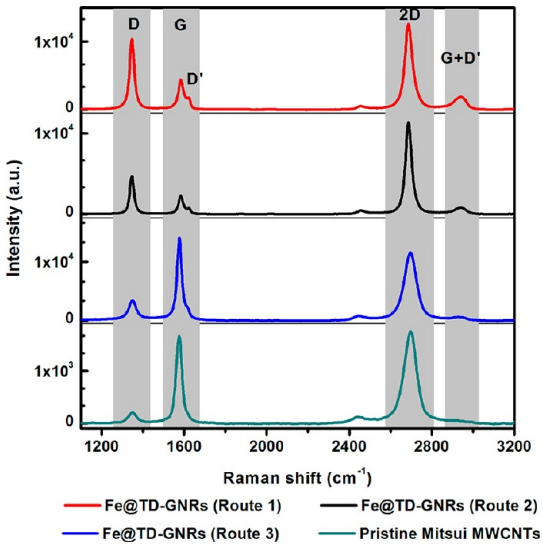

Figure 4. Raman spectra of Fe@TD-GNRs synthesized using routes 1 (red), 2 (black), and 3 (blue) and pristine Mitsui MWCNTs (dark green). Gray rectangles represent different vibrational mode regions.

oxygen, was also monitored. Although an argon atmosphere was used, oxygen is always present in low concentrations that can be detected by the mass analyzer. The analysis indicates that oxygen is consumed during the region IV process. This might indicate that fragments, corresponding to alkyl chains, are partially burning. A similar oxygen consumption was present in region II at 475 °C; such consumption stops and reappears at 700 °C in region IV. Since 700 °C is a rather high temperature for normal combustion, it might be due to iron interactions with jagged edges of the graphene. However, the actual process in region IV remains unclear. The control EGA experiment with pristine Mitsui MWCNTs was recorded, and no gases characteristic of alkyl groups were evolved during thermolysis (Supporting Information Figure S1).

Raman Spectroscopy. Comparison of Raman spectra revealed interesting differences between Fe@TD-GNRs synthesized by routes 1, 2, or 3 (Figure 4). One difference is the peak position for Fe@TD-GNR materials. Materials synthesized using routes 1 and 2 have the following peak positions: D peak, 1347 cm^{-1}; G peak, 1584 cm^{-1}; and 2D peak, 2687 cm^{-1}; while materials synthesized according to route 3 and pristine Mitsui MWCNTs have the following peak positions: D peak, 1350 cm^{-1}; G peak, 1575 cm^{-1}; and 2D peak, 2697 cm^{-1}. The second difference is the appearance of the G + D′ peak at 2938 cm^{-1} for Fe@TD-GNRs synthesized using routes 1 and 2. However, the most obvious difference between the products is the ratio of the intensity of the D band to the G band (I_D/I_G ratio). The I_D/I_G ratio is considered a measure of the structural disorder of the material.[25] Fe@TD-GNRs synthesized according to routes 1 and 2 show a reversed I_D/I_G ratio; 1.82 and 1.60, respectively, compared to Fe@TD-GNRs synthesized

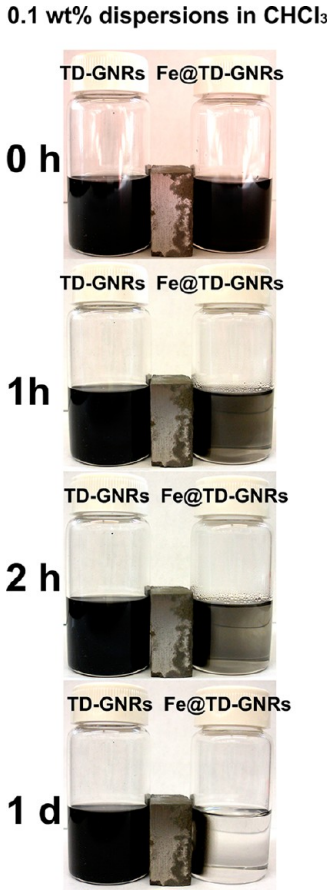

Figure 5. Comparison of solubility and magnetization in the presence of a bar magnet (magnetic field strength 0.3 T) of 0.1 wt % TD-GNRs (left column) and 0.1 wt % Fe@TD-GNRs (right column), noted over a period of 1 day.

according to route 3 and pristine Mitsui MWCNTs, with I_D/I_G of 0.4 and 0.16, respectively. This suggests that significant system disorder was induced by intercalation of $FeCl_3$ directly into the tubular graphitic structure of MWCNTs (routes 1 and 2). The disorder was not as obvious when $FeCl_3$ was intercalated into the GNRs (route 3).

Bulk Properties. It is of great importance for materials to be dispersible or soluble, thereby affording processability. We have focused on the dispersion of high-iron-content Fe@TD-GNRs synthesized according to route 3 since the products from route 1 and route 2 exhibited weaker magnetic response due to lower iron concentration. The tetradecyl groups on the edges of Fe@TD-GNRs greatly improved the solubility of the ribbons (Supporting Information Figure S2). After weeks, Fe@TD-GNRs at 0.1 wt % dispersions in chloroform and chlorobenzene retained relatively good solution stability. To show the magnetization properties of Fe@TD-GNRs in the presence of a magnetic field, 0.1 wt % solution of Fe@TD-GNRs in chloroform was exposed to a fixed (bar) magnetic field with a field strength of 0.3 T. For comparison, TD-GNRs with no intercalated iron were exposed to the same magnetic field.

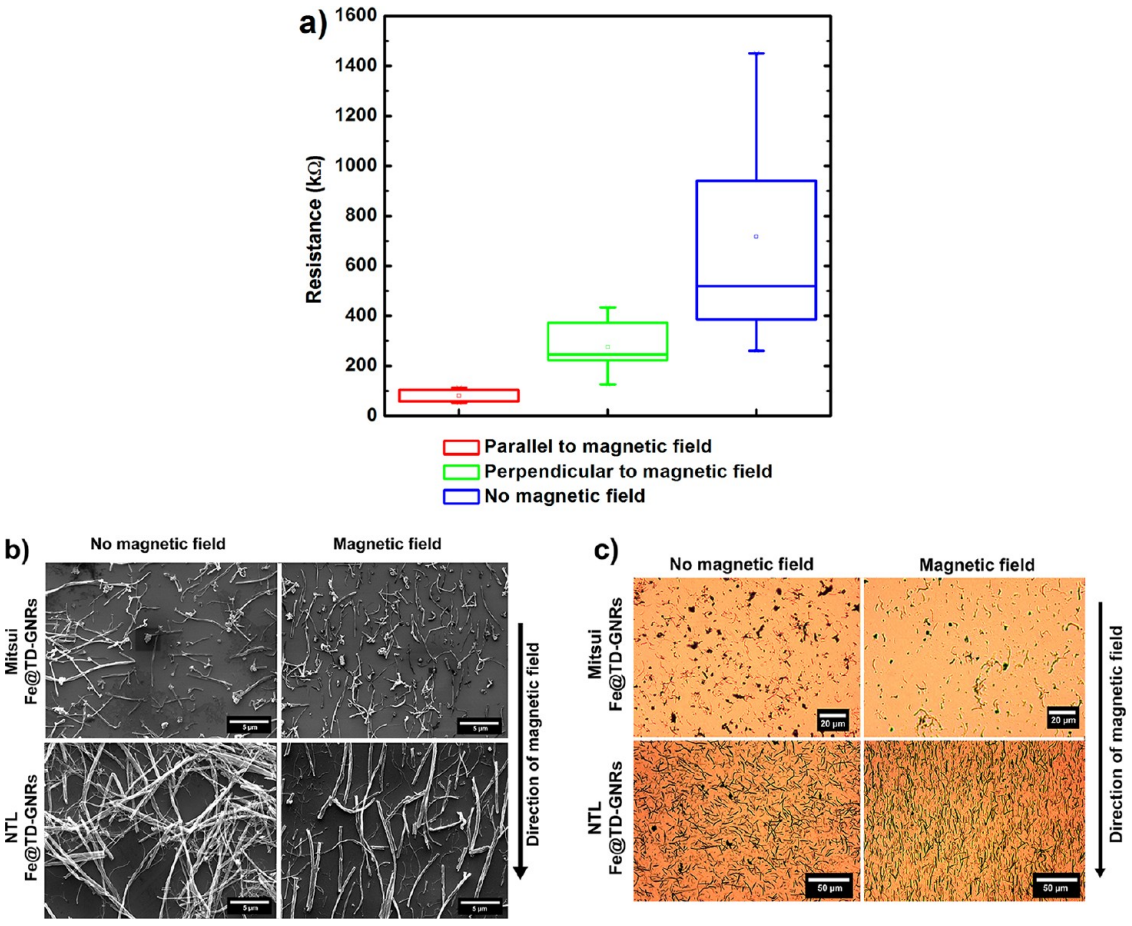

Figure 6. Behavior of Fe@TD-GNRs in a 0.3 T magnetic field. (a) Resistance of 5 wt % suspension of Fe@TD-GNRs synthesized according to route 3 in a commercially available mixture of hydrocarbons (diesel fuel). The red box in the chart represents resistance measured parallel to the magnetic field; the green box represents the resistance measured perpendicular to the magnetic field, and the blue box represents the resistance measured outside of the magnetic field. Results are presented statistically. The box was determined by the 25th and 75th percentiles; the spread lines are determined by the 5th and 95th percentiles, and the mean value is denoted by a square symbol inside each box. Each measurement was taken after 2 min of system perturbation. A permanent laboratory magnet was used (for setup, please see Supporting Information). (b) SEM images of Mitsui- and NTL-originated Fe@TD-GNRs. Suspensions of Fe@TD-GNRs in chlorobenzene were drop-cast onto a SiO_2/Si substrate and dried inside of a magnetic field (right two images). For comparison, the left two images are solutions that were dried outside of a magnetic field. All scale bars are 5 μm. (c) Optical microscope images of Mitsui- and NTL-originated Fe@TD-GNRs drop-cast onto a glass substrate and dried outside of a magnetic field (left two images). For comparison, the right two images are solutions that were dried inside of a magnetic field.

The difference is evident (Figure 5). Suspensions with intercalated iron become clear after 2 h due to a phase separation. Conversely, suspensions with no intercalated iron remain black, and no separation occurs.

As discussed previously, for applications in energy-related devices, transparent touch screens, carbon fiber spinning and coating, polymer composites, and various drilling, completion, and logging fluids, it is advantageous if the carbon materials are easily processable and adequately conductive. Processability often requires solubility or dispersibility in various solvents. It has been shown that the Fe@TD-GNRs form stable suspensions in organic solvents. While single ribbon conductivity has been reported previously,[7] the bulk conductivity of the materials is important for several applications and is directly correlated to electrical percolation at a constant concentration. To test the hypothesis that electrical percolation at a given concentration can be improved by aligning anisotropic Fe@TD-GNRs in the presence of a magnetic field, a simple testing cell was designed (Supporting Information Figure S3). The testing cell was fabricated to simultaneously measure resistance of a 5 wt % solution of Fe@TD-GNRs in a commercially available mixture of hydrocarbons (diesel fuel as commonly used in commercial conductive fluid) both parallel and perpendicular to a magnetic field. A control experiment without a magnetic field was also used. The results confirmed the hypothesis (Figure 6a). The resistance, which is related to electrical percolation, was ~80 kΩ when it was measured parallel to the magnetic field. In this direction, anisotropic Fe@TD-GNRs are aligned along the longer side of the GNRs. When the resistance of the suspension was measured perpendicular to the

magnetic field, the value increased by a factor of 3.5 to ~275 kΩ. As a control experiment, the measurement of the resistance outside of the magnetic field showed a resistance of ~720 kΩ, which is almost 10 times higher than for the aligned Fe@TD-GNR solution. Additionally, statistics revealed another interesting feature of the suspension. The distribution of results was narrow for measurements parallel to the magnetic field, while measurements outside of the magnetic field yielded a very wide distribution. This is an indication that, when Fe@TD-GNRs are exposed to a magnetic field, a similar carbon arrangement for electrical percolation is produced. When the resistances of Fe@TD-GNR suspensions are measured outside of the magnetic field, the electrical percolation and GNR arrangement are ill-defined, thus the distribution is wider.

Scanning electron microscope (SEM) (Figure 6b) and optical microscope images (Figure 6c) of magnetically (bar) aligned and randomly arranged Fe@TD-GNRs, produced both from Mitsui and NanoTechLabs (NTL) MWCNTs, were recorded. The NTL Fe@TD-GNRs were synthesized using the same procedure (route 3) as those Fe@TD-GNRs produced from Mitsui MWCNTs, and they have similar bulk, EGA, XPS, and Raman properties. The only difference between Mitsui and NTL Fe@TD-GNRs is that NTL Fe@TD-GNRs possess up to 6 wt % iron from the starting MWCNT synthesis process. However, the concentration of iron increased significantly during route 3, up to 27 wt %, to make the NTL Fe@TD-GNRs, indicating the additional intercalation of iron. These images (Figure 6b,c) clearly show the magnetic-field-induced alignment of the Fe@TD-GNRs that is possible, thereby explaining the reduced resistance observed for the magnetically treated suspension (Figure 6a).

Therefore, the magnetically enhanced alignment resulting in enhanced conductivity has been clearly observed. This could spawn advances in numerous applications ranging from conductive displays to conductive fluids.

CONCLUSIONS

It has been shown that commercially available MWCNTs can be *in situ* split and functionalized, yielding organic solvent-soluble GNR stacks with preserved conductivity.[14] In the present study, iron has been intercalated between edge-functionalized graphene nanoribbon stacks to make Fe@TD-GNRs. The intercalated iron was imaged by TEM. The synthesis route was optimized to enhance iron concentration. Iron content was estimated with TGA and XPS. TGA revealed iron contents as high as 29.5 wt %, while iron concentrations up to 4.4 wt % for the same material were estimated by XPS. The discrepancy between the TGA and XPS results can be an indirect indication of intercalation, as XPS analyzes predominantly surface iron. EGA produced four different temperature regions in which fragments were extruded from the product. The first three correspond to regions noted in our previous studies and are most likely a reflection of deintercalation and defunctionalization of hydrocarbons and alkyl groups, respectively. The unusually high-temperature region IV, however, is unique and appears to be characteristic of iron-intercalated GNRs. Raman spectroscopy revealed reversed I_D/I_G ratio for samples synthesized by the different routes. Fe@TD-GNRs synthesized according to route 3 had similar Raman spectra with similar I_D/I_G ratio as starting material Mitsui MWCNTs. Products synthesized according to routes 1 and 2 showed reversed I_D/I_G ratio compared to route 3, indicating that the structure derived using route 3 is more ordered with respect to the graphene planes. Anisotropy together with magnetization enabled directional alignment of Fe@TD-GNRs in a magnetic field. SEM images in the magnetic field showed alignment. Moreover, 5 wt % suspension of Fe@TD-GNRs in hydrocarbons exposed to a magnetic field showed enhanced electrical percolation, as the resistance was lower than that of material exposed to no magnetic field. Further, the narrow distribution of results for aligned suspensions might be an indication of an ordered percolation architecture in these suspensions compared to the wide distribution for randomly formed percolation produced in non-aligned suspensions. Enhanced electrical percolation, solubility, and conductivity present in one material could be of interest for energy-related devices, transparent touch screens, carbon fiber spinning and coating, polymer composites, and various commercial conductive fluids. Achieving enhanced electrical percolation at a given concentration could have an impact on volume and mass capacity of energy-related devices such as in Li-ion batteries or ultracapacitors.

EXPERIMENTAL SECTION

Materials. Reactions were performed in dried glassware under a N_2 atmosphere unless stated otherwise. Reagent-grade 1,2-DME was degassed with Ar, refluxed over sodium in a N_2 atmosphere, and freshly distilled. Other solvents were used without further purification. Mitsui MWCNTs were received from Mitsui & Co. (lot no. 05072001K28). NTL-M-grade MWCNTs were donated by Nanotech Laboratories, Inc. (5T10M10). All other commercially available reagents were used as received. Liquid Na/K alloy was prepared in a vial inside a N_2 glovebox by pressing together freshly cut K (1 molar equiv) and Na (0.22 molar equiv) chunks using tweezers to facilitate the melting process. Amounts of liquid Na/K alloy are indicated by volume. *Caution: All synthetic steps involving Na/K alloy should be carried out with extreme caution under strict exclusion of air and moisture, under inert gas and appropriate personal protection (hood, blast shields, face shield, protective and fire resistant clothing) should be used at all times.* 1-Iodotetradecane was obtained from Eastman and used as received.

In-house deionized water was used during purification of the products.

Synthesis of Fe@TD-GNRs. Detailed synthesis procedure of Fe@TD-GNRs synthesized according to route 1 and route 2 are part of Supporting Information. **Route 3.** To an oven-dried 250 mL round-bottom flask containing a magnetic stir bar was added MWCNTs (100 mg, 8.3 mmol). The vessel was transferred to a N_2 glovebox where freshly distilled 1,2-DME (35 mL) and liquid Na/K alloy (0.29 mL) were added. The flask with the suspension was sealed with septa and transferred out of the glovebox, where the suspension was dispersed by a short 5 min ultrasonication (using ultrasonic cleaner Cole-Parmer model 08849-00) to yield a dark greenish to red suspension. After ultrasonication, the reaction mixture was vigorously stirred (450 rpm) at room temperature for 3 days. The reaction suspension was then quenched by the addition of methanol (20 mL, 500 mmol) using a syringe, and stirring was continued at room temperature for 10 min. The reaction mixture was filtered over a 0.45 μm pore size PTFE membrane. The filter cake was successively washed with THF (100 mL), *i*-PrOH (100 mL), H_2O (100 mL), *i*-PrOH (20 mL), THF (20 mL), and Et_2O (10 mL). The filter cake was then dried in vacuum ($\sim 10^{-2}$ Torr) for 24 h. The resulting nonfunctionalized GNRs (100 mg) and $FeCl_3$ (300 mg) were charged into a two-zone glass ampule separately. The ampule was evacuated and sealed under vacuum using an acetylene torch. The loaded and sealed ampule was inserted into a muffle furnace (NEY 6-160A) and heated at 350 °C for 24 h. The cooled ampule was transferred to a glovebox and opened. The intercalated and partially split carbon material was transferred into an oven-dried 250 mL round-bottom flask containing a magnetic stir bar, and freshly distilled 1,2-DME (35 mL) and liquid Na/K alloy (0.29 mL) were added. The flask containing the suspension was sealed with a septum and transferred out of the glovebox, where the suspension was dispersed by a short 5 min ultrasonication (using ultrasonic cleaner Cole-Parmer model 08849-00) to yield a dark greenish to red suspension. After ultrasonication, the reaction mixture was vigorously stirred (450 rpm) at room temperature for 7 h. The reaction suspension was then quenched by the addition of the 1-iodotetradecane (2.84 g, 2.44 mL, 8.75 mmol) using a syringe and left to stir at the room temperature for an additional 24 h. Methanol (20 mL, 500 mmol) was added to quench any excess Na/K alloy, and the mixture was stirred at room temperature for 10 min. For workup, the reaction mixture was filtered over a 0.45 μm pore size PTFE membrane. The filter cake was successively washed with THF (100 mL), *i*-PrOH (100 mL), H_2O (100 mL), *i*-PrOH (100 mL), THF (100 mL), and Et_2O (10 mL). The product was then dried in vacuum ($\sim 10^{-2}$ Torr) for 24 h.

Thermogravimetric Analysis (TGA). TGA was performed on TA Q50 instrument at a heating rate of 10 °C/min, from room temperature to 900 °C. The experiment was carried out under an air atmosphere at a flow rate of 40.0 mL/min.

X-ray Photoelectron Spectroscopy (XPS). XPS was carried out on a PHI Quantera SXM scanning X-ray microscope. As an X-ray source, an Al anode at 25 W was used with a pass energy of 26.00 eV, 45° takeoff angle, and a 100 μm beam size. A pass energy of 140 eV was used for survey and 26 eV for atomic concentration.

Electron and Optical Microscopy. Samples were dispersed in chloroform and bath sonicated using an ultrasonic cleaner (Cole-Parmer model 08849-00) for 15 min for a quick dispersion. The suspension was drop-cast on a 100 nm SiO_2/Si substrate, and large-area low-resolution images were taken at 20 kV using a FEI Quanta 400 ESEM FEG scanning electron microscope and under a JEOL-6500 field-emission microscope. For more refined images of the ribbon structure at higher resolution, a JEOL 2010 transmission electron microscope (JEOL 2010-TEM) was used with the sample prepared on a coated TEM grid as above. For optical microscopy, the material was examined on a glass substrate and imaged on a polarizing optical microscope (Zeiss Axio).

Evolved Gas Analysis (EGA). EGA measurements were performed using a Netzsch 449 F3 Jupiter TGA instrument under a dynamic Ar flow with a flow rate of 60 mL/min in a temperature range from 25 to 900 °C. A heating rate of 10 °C/min was used. About 5 mg of sample was placed in an alumina (Al_2O_3) crucible. Simultaneously, mass spectrometry was performed on a MS 403C Aëolos with SEM Chenneltron detector and system pressure of 2×10^{-5} Torr. Gases evolved under TGA heat treatment were transferred to the mass spectrometer through a transfer capillary (quartz, 75 μm i.d.) that was heated at 220 °C. The upper limit of the mass spectrometer detector was 100 amu.

Raman Spectroscopy. Raman spectra of powder samples of the functionalized GNRs and MWCNTs were recorded with an InVia Renishaw microscope using a 514.5 nm argon laser. The areas of the D to G bands on the spectrum were integrated, and a Lorentz fit was applied to the spectra to accurately determine the ratio of the D to G bands.

Conductivity Measurements. Resistance was measured using a Fluke 79 III True RMS multimeter. For the setup, see Supporting Information.

Conflict of Interest: The authors declare no competing financial interest.

Acknowledgment. We thank MI-SWACO, the Advanced Energy Consortium (BG Group, Halliburton, Conoco Phillips, bp, OXY, Marathon, Shell, Total, Petrobras, Schlumberger), the AFOSR (FA9550-09-1-0581), Center of Excellence Low Carbon Technologies, Slovenia (CO NOT), Center of Excellence Advanced Materials and Technologies for the Future, Slovenia (CO NAMASTE), the Lockheed Martin Corporation through the LANCER IV Program, the AFOSR MURI (FA9550-12-1-0035), and the ONR MURI program (#00006766, N00014-09-1-1066) for funding. We thank Drs. A. Tanioka and M. Endo for the donation of the Mitsui MWCNTs, and Nanotech Laboratories, Inc. for the NTL MWCNTs.

Supporting Information Available: Additional EGA of MWCNTs, solubility tests, schematics of the developed testing cell with magnet setup and detailed synthesis of Fe@TD-GNRs according to route 1 and route 2. This material is available free of charge *via* the Internet at http://pubs.acs.org.

REFERENCES AND NOTES

1. Geim, A. K. Graphene: Status and Prospects. *Science* **2009**, *324*, 1530–1534.
2. Luo, B.; Liu, S.; Zhi, L. Chemical Approaches toward Graphene-Based Nanomaterials and Their Applications in Energy-Related Areas. *Small* **2012**, *8*, 630–646.
3. Zhu, Y.; Sun, Z.; Yan, Z.; Jin, Z.; Tour, J. M. Rational Design of Hybrid Graphene Films for High-Performance Transparent Electrodes. *ACS Nano* **2011**, *5*, 6472–6479.
4. Xiang, C.; Lu, W.; Zhu, Y.; Sun, Z.; Yan, Z.; Hwang, C.-C.; Tour, J. M. Carbon Nanotube and Graphene Nanoribbon-Coated Conductive Kevlar Fibers. *ACS Appl. Mater. Interfaces* **2012**, *4*, 131–136.
5. Asquith, G. B.; Krygowski, D. *Basic Well Log Analysis: AAPG Methods in Exploration No. 16*, 2nd ed.; American Association of Petroleum Geologists: Tulsa, OK, 2004; p 244.
6. Li, X.; Wang, X.; Zhang, L.; Lee, S.; Dai, H. Chemically Derived, Ultrasmooth Graphene Nanoribbon Semiconductors. *Science* **2008**, *319*, 1229–1232.
7. Kosynkin, D. V.; Lu, W.; Sinitskii, A.; Pera, G.; Sun, Z.; Tour, J. M. Highly Conductive Graphene Nanoribbons by Longitudinal Splitting of Carbon Nanotubes Using Potassium Vapor. *ACS Nano* **2011**, *5*, 968–974.
8. Kosynkin, D. V.; Higginbotham, A. L.; Sinitskii, A.; Lomeda, J. R.; Dimiev, A.; Price, B. K.; Tour, J. M. Longitudinal Unzipping of Carbon Nanotubes To Form Graphene Nanoribbons. *Nature* **2009**, *458*, 872–876.
9. Cano-Márquez, A. G.; Rodríguez-Macías, F. J.; Campos-Delgado, J.; Espinosa-González, C. G.; Tristán-López, F.; Ramírez-González, D.; Cullen, D. A.; Smith, D. J.; Terrones, M.; Vega-Cantú, Y. I. Ex-MWNTs: Graphene Sheets and Ribbons Produced by Lithium Intercalation and Exfoliation of Carbon Nanotubes. *Nano Lett.* **2009**, *9*, 1527–1533.
10. Jiao, L.; Zhang, L.; Wang, X.; Diankov, G.; Dai, H. Narrow Graphene Nanoribbons from Carbon Nanotubes. *Nature* **2009**, *458*, 877–880.

11. Wang, J.; Ma, L.; Yuan, Q.; Zhu, L.; Ding, F. Transition-Metal-Catalyzed Unzipping of Single-Walled Carbon Nanotubes into Narrow Graphene Nanoribbons at Low Temperature. *Angew. Chem., Int. Ed.* **2011**, *50*, 1–6.
12. Shinde, D. B.; Debgupta, J.; Kushwaha, A.; Aslam, M.; Pillai, V. K. Electrochemical Unzipping of Multi-walled Carbon Nanotubes for Facile Synthesis of High-Quality Graphene Nanoribbons. *J. Am. Chem. Soc.* **2011**, *133*, 4168–4171.
13. Talyzin, A. V.; Anoshkin, I. V.; Krasheninnikov, A. V.; Nieminen, R. M.; Nasibulin, A. G.; Jiang, H.; Kauppinen, E. I. Synthesis of Graphene Nanoribbons Encapsulated in Single-Walled Carbon Nanotubes. *Nano Lett.* **2011**, *11*, 4352–4356.
14. Genorio, B.; Lu, W.; Dimiev, A. M.; Zhu, Y.; Raji, A.-R. O.; Novosel, B.; Alemany, L. B.; Tour, J. M. *In Situ* Intercalation Replacement and Selective Functionalization of Graphene Nanoribbon Stacks. *ACS Nano* **2012**, *6*, 4231–4240.
15. Bauhofer, W.; Kovacs, J. Z. A Review and Analysis of Electrical Percolation in Carbon Nanotube Polymer Composites. *Compos. Sci. Technol.* **2009**, *69*, 1486–1498.
16. Du, F.; Fischer, J. E.; Winey, K. I. Effect of Nanotube Alignment on Percolation Conductivity in Carbon Nanotube/Polymer Composites. *Phys. Rev. B* **2005**, *72*, 1–4.
17. Kunstmann, J.; Özdoğan, C.; Quandt, A.; Fehske, H. Stability of Edge States and Edge Magnetism in Graphene Nanoribbons. *Phys. Rev. B* **2011**, *83*, 1–8.
18. Ericson, L. M.; Fan, H.; Peng, H.; Davis, V. A.; Zhou, W.; Sulpizio, J.; Wang, Y.; Booker, R.; Vavro, J.; Guthy, C.; *et al.* Macroscopic, Neat, Single-Walled Carbon Nanotube Fibers. *Science* **2004**, *305*, 1447–1450.
19. Correa-Duarte, M. A; Grzelczak, M.; Salgueiriño-Maceira, V.; Giersig, M.; Liz-Marzan, L. M.; Farle, M.; Sierazdki, K.; Diaz, R. Alignment of Carbon Nanotubes under Low Magnetic Fields through Attachment of Magnetic Nanoparticles. *J. Phys. Chem. B* **2005**, *109*, 19060–19063.
20. Ebert, L. B. Intercalation Compounds of Graphite. *Annu. Rev. Mater. Sci.* **1976**, *6*, 181–211.
21. Dresselhaus, M. S.; Dresselhaus, G. Intercalation Compounds of Graphite. *Adv. Phys.* **2002**, *51*, 1–186.
22. Kalucki, K.; Morawski, A. W. Iron Intercalated in Graphite as Catalysts for Ammonia Synthesis. *J. Chem. Technol. Biotechnol.* **1990**, *47*, 357–363.
23. Mordkovich, V. Z.; Baxendale, M.; Chang, R. P. H.; Yoshimura, S. Intercalation into Carbon Nanotubes without Breaking the Tubular Structure. *Synth. Met.* **1997**, *86*, 2049–2050.
24. Hellman, H.; Laitinen, R. S.; Kaila, L.; Jalonen, J.; Hietapelto, V.; Jokela, J.; Sarpola, A.; Ramo, J. Identification of Hydrolysis Products of $FeCl_3 \cdot 6H_2O$ by ESI-MS. *J. Mass Spectrom.* **2006**, *41*, 1421–1429.
25. Nakamizo, M.; Kammereck, R.; Walker, P. L. Laser Raman Studies on Carbons. *Carbon* **1974**, *12*, 259–267.